

Novel spectral range expansion method for liquid crystal adaptive optics

Quanquan Mu, Zhaoliang Cao,* Lifa Hu, Yonggang Liu, Zenghui Peng, and Li Xuan

State Key Laboratory of Applied Optics, Changchun Institute of Optics, Fine Mechanics and Physics,
Chinese Academy of Sciences, Changchun, Jilin 130033 China

*caozlok@ciomp.ac.cn

Abstract: Energy loss is a main problem of liquid crystal adaptive optics systems (LC AOSs). It is caused by the polarization dependence and narrow spectral range. The polarization dependence has been avoided by Love and Mu et al. [Appl. Opt. **32**, 2222 (1993); Appl. Opt. **47**, 4297 (2008)]. In this paper, a novel method was proposed to extend the spectral range of LC AOSs using multiple liquid crystal wavefront correctors (LCWFCs) to improve the energy utilization. Firstly, the chromatism of an LCWFC was measured and analyzed. The calculated results indicate that one LCWFC is only suitable to perform adaptive correction for a narrow waveband; therefore, multiple LCWFCs must be used to achieve a broadband correction. Secondly, based on open-loop control, a novel optical layout consisting of three LCWFCs was proposed to extend the spectral range of LC AOSs and thus achieve correction in the whole waveband of 520–810 nm. Thirdly, a broadband correction experiment was conducted and near diffraction-limited resolution was achieved in the waveband of 520–690 nm. Finally, a 500 m horizontal turbulence correction experiment was performed in the waveband of 520–690 nm. With adaptive correction, the resolution of the optical system was improved significantly and the image of the single fiber was clearly resolved. Furthermore, compared with a sub-waveband system, the system energy was improved. The energy of the whole waveband is equal to the sum of all the sub-wavebands. The experiment results validated our method and indicate that the chromatism in a broad waveband of LC AOSs can be eliminated. And then, the system energy can be improved greatly using the novel method.

© 2010 Optical Society of America

OCIS codes: (010.1080) Adaptive optics; (230.3720) Liquid-crystal devices; (010.1285) Atmospheric correction.

References and links

1. Z. Cao, Q. Mu, L. Hu, D. Li, Y. Liu, L. Jin, and L. Xuan, "Correction of horizontal turbulence with nematic liquid crystal wavefront corrector," *Opt. Express* **16**(10), 7006–7013 (2008).
2. G. D. Love, "Wave-front correction and production of Zernike modes with a liquid-crystal spatial light modulator," *Appl. Opt.* **36**(7), 1517–1520 (1997).
3. S. Restaino, D. Dayton, S. Browne, J. Gonglewski, J. Baker, S. Rogers, S. McDermott, J. Gallegos, and M. Shilko, "On the use of dual frequency nematic material for adaptive optics systems: first results of a closed-loop experiment," *Opt. Express* **6**(1), 2–6 (2000).
4. M. A. A. Neil, M. J. Booth, and T. Wilson, "Dynamic wave-front generation for the characterization and testing of optical systems," *Opt. Lett.* **23**(23), 1849–1851 (1998).
5. G. D. Love, "Liquid-crystal phase modulator for unpolarized light," *Appl. Opt.* **32**(13), 2222–2223 (1993).
6. G. D. Love, S. R. Restaino, R. C. Carreras, G. C. Loos, R. V. Morrison, T. Baur, and G. Kopp, "Polarization insensitive 127-segment liquid crystal wavefront corrector," *OSA summer topical meeting on adaptive optics*, p. 288–290 (1996).
7. Q. Mu, Z. Cao, D. Li, L. Hu, and L. Xuan, "Open-loop correction of horizontal turbulence: system design and result," *Appl. Opt.* **47**(23), 4297–4301 (2008).
8. S. Serati, and J. Stockley, "Advances in liquid crystal based devices for wavefront control and beamsteering," *Proc. SPIE* **5894**, 58940K (2005).
9. J. E. Stockley, G. D. Sharp, S. A. Serati, and K. M. Johnson, "Analog optical phase modulator based on chiral smectic and polymer cholesteric liquid crystals," *Opt. Lett.* **20**(23), 2441–2443 (1995).

10. Z. Cao, L. Xuan, L. Hu, Y. Liu, and Q. Mu, "Effects of the space-bandwidth product on the liquid-crystal kinoform," *Opt. Express* **13**(14), 5186–5191 (2005).
 11. A. K. Kirby, and G. D. Love, "Fast, large and controllable phase modulation using dual frequency liquid crystals," *Opt. Express* **12**(7), 1470–1475 (2004).
 12. G. D. Love, A. K. Kirby, and R. A. Ramsey, "Sub-millisecond, high stroke phase modulation using polymer network liquid crystals," *Opt. Express* **18**(7), 7384–7389 (2010).
 13. V. Laude, "Twisted nematic liquid-crystal pixelated active lens," *Opt. Commun.* **153**(1-3), 134–152 (1998).
-

1. Introduction

Liquid crystal wavefront correctors (LCWFCs), which are used to match the spatial resolution demand of large aperture telescopes, have been widely investigated [1–4]. However, compared with deformable mirrors, LCWFC has the critical drawback of low light efficiency due to its polarization dependence and narrow spectral range. Love et al. proposed two methods to solve the polarization dependence problem [5,6]. Mu et al. proposed another method of using a polarized beam splitter (PBS) to solve the problem [7]. Aside from polarization dependence, the narrow working spectral range of liquid crystal adaptive optics systems (LC AOSs) contributes to the energy loss. Recently, Stockley demonstrated that non-dispersive LCWFCs can be obtained by utilizing chiral smectic ferroelectric liquid crystals [8,9]. However, this kind of LCWFC has limitations. One, the quantified phase level is low, which will reduce the correction accuracy. Two, incident light with a circular polarization must be used. Three, the amplitude of the light is modulated at a specific broadband. Lastly, manufacturing such an LCWFC is not easy. In this paper, a parallel correction technique with multi-LCWFCs is suggested to expand the spectral range of LC AOSs.

To correct atmospheric turbulence, the response speed of the liquid crystal (LC) should be extremely high. As the response speed is proportional to the square of the LC thickness, the LC thickness should be as slight as possible to obtain higher response speed. However, thinner LC produces lesser phase modulation. Therefore, a phase wrapping method is presented to achieve larger phase modulation and faster response [10]. Using this method, an LCWFC with the phase modulation of 2π can produce several, even tens of microns modulation magnitude. The distortion magnitude of the atmospheric turbulence is normally several microns. Thus, the phase wrapping method is very suitable and essential in correcting atmospheric turbulence. Of course, dual-frequency LCs can directly obtain larger phase modulation with fast response [11]. However, dual-frequency LCs needs higher driving voltage, and then the very large scale integration (VLSI) technique cannot be used to drive this kind of LC. Therefore, the active element number is very little and the advantage of the LC WFC is lost. Furthermore, polymer network LC was considered to acquire large phase stroke and fast response [12]. But, the phase stroke is only 2λ ($\lambda = 633\text{nm}$), which is not suitable to correct the atmospheric turbulence. Meanwhile, because of the effect of the polymer network, the driving voltage is high. Consequently, we only considered the LCWFC that is used with the phase wrapping method in this paper.

Theoretically, LCWFC is only suitable to be used for wavefront correction for a single wavelength and not on a waveband due to chromatism. However, if a minor error is allowed, LCWFC can be used to correct the distortion in a narrow spectral range. To fulfill this purpose, the chromatism effect on the correction accuracy of LCWFC should be analyzed. The chromatism of LCWFC includes refractive index chromatism and quantization chromatism. Refractive index chromatism is caused by the LC material and is generally called dispersion. Meanwhile, the quantization chromatism is caused by modulo 2π of phase wrapping. In addition, atmospheric turbulence and the optical system are capable of chromatism. Since the chromatism of the atmospheric turbulence is slight and the optical system is achromatic, both were disregarded in this paper.

2. Effects of chromatism on the diffraction efficiency of LCWFC

To analyze the dispersion of the LC material, a nematic LC material (RDP-92975, DIC) was injected into a parallel-aligned cell, and the birefringence Δn was measured using a spectroscopic ellipsometer (JOBIN YVON). The measured birefringence dispersion curve is

shown in Fig. 1. It can be seen that the birefringence Δn is dependent on the wavelength and the dispersion of the LC material is particularly severe when the wavelength is less than 500 nm. In this instance, we are trying to achieve a broadband correction with an acceptable variation of Δn . Since a phase wrapping technique is used, the phase distribution should be modulo 2π , and it should then be quantized [10]. Assuming that the quantization wavelength is λ_0 , the thickness of the LC layer is d , and V_{max} denotes the voltage needed to obtain a 2π phase modulation, and then the maximum phase modulation of the LCWFC can be expressed as

$$\Delta\varphi_{max}(\lambda_0) = 2\pi \frac{\Delta n(\lambda_0, V_{max})d}{\lambda_0} = 2\pi. \quad (1)$$

For any other wavelength λ , it can be rewritten as

$$\Delta\varphi_{max}(\lambda) = 2\pi \frac{\Delta n(\lambda, V_{max})d}{\lambda}. \quad (2)$$

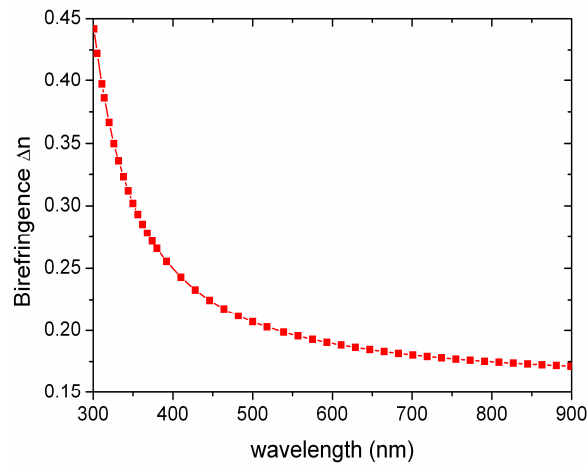


Fig. 1. Birefringence Δn as a function of wavelength, measured by a spectroscopic ellipsometer.

From Eq. (2), we can see that the phase modulation error will be generated due to the variations of Δn and λ . Equation (2) and the measured data shown in Fig. 1 were used to calculate the effects of Δn and λ on $\Delta\varphi_{max}$ were calculated. For quantization wavelength of 550 nm, 633 nm and 750 nm, the variation of maximum phase modulation as a function of wavelength is shown in Fig. 2. Assuming the deviation of the phase modulation is 0.1, for $\lambda_0 = 550, 633$ and 750 nm, the corresponding spectral ranges were calculated as 520–590 nm, 590–690 nm and 690–810 nm, respectively. If a 10% phase modulation error is acceptable, then the LCWFC only can be used to correct the distortion for a finite spectral range.

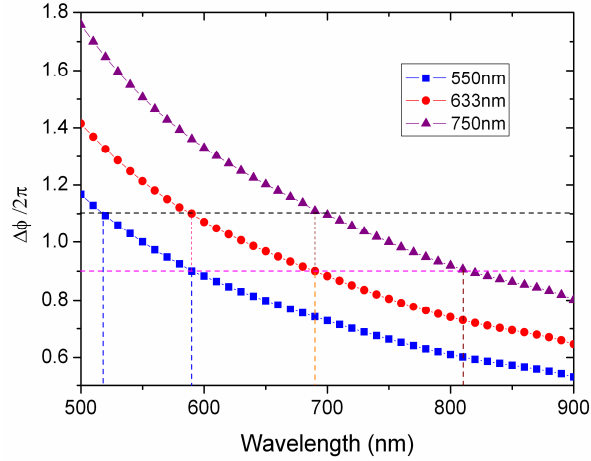


Fig. 2. Phase modulation as a function of wavelength for $\lambda_0 = 550$ nm, 633 nm, and 750 nm, respectively; the two horizontal dashed lines indicate the phase deviation range; while the four vertical dashed lines illustrate three sub-wavebands of 520–590 nm, 590–690 nm and 690–820 nm, respectively.

The variation of Δn and λ affects the diffraction efficiency of the LCWFC. Using the Fresnel phase lens model, the diffraction efficiency for any other wavelength λ can be described as [13]

$$\eta = \left| \frac{\sin(\pi d \Delta n(\lambda, V_{\max}) / \lambda)}{\pi(d \Delta n(\lambda, V_{\max}) / \lambda - 1)} \right|^2. \quad (3)$$

The effects of Δn and λ on the diffraction efficiency are shown in Fig. 3. For $\lambda_0 = 550$ nm, 633 nm, and 750 nm and their respective corresponding wavebands of 520–590 nm, 590–690 nm, and 690–810 nm, the maximum energy loss is 3%, which is acceptable for the LC AOS. Although only one kind of LC material was measured and analyzed in this work, the calculated results are helpful in the usage of LCWFCs because almost all the nematic LC materials have similar dispersion characteristic.

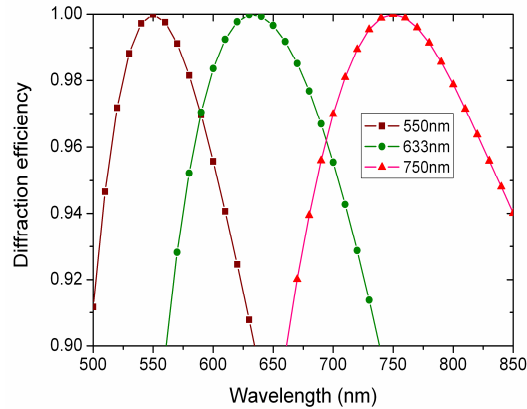


Fig. 3. Diffraction efficiency as a function of wavelength for $\lambda_0 = 550$ nm, 633 nm, and 750 nm, respectively.

3. Broadband correction with multi-LCWFCs

3.1 Realization method

The above calculated results show that it is only possible to correct the distortion in a narrow waveband using only one LCWFC. Therefore, to realize the distortion correction in a broadband of 520–810 nm, three LCWFCs are necessary; each LCWFC is responsible for the correction of different wavebands and then three corrected beams are combined to realize the correction in the whole waveband. The proposed optical set-up is shown in Fig. 4, where a PBS is used to split the unpolarized light into two linear polarized beams. One beam is used to measure the distortion by using a wavefront sensor (WFS), while the other goes to the LCWFC. The LC AOS must be controlled through the open-loop method, the detailed description of which can be found in Ref.7. Three dichroic beam splitters (DBSs) are used to acquire different wavebands. A 520–810 nm waveband is acquired by using a bandpass filter (DBS1). This broadband beam is then divided into two beams by a long-wave pass filter (DBS2). Since DBS2 has a cutoff point of 590 nm, the reflected and transmitted beams of DBS2 have wavebands of 520–590 nm and 590–820 nm, respectively. The transmitted beam is then split once more by another long-wave pass filter (DBS3) whose cutoff point is 690 nm. Through DBS3, the reflected and transmitted beams acquire wavebands of 590–690 nm and 690–810 nm, respectively. Thus, the broadband beam of 520–810 nm is divided into three sub-wavebands, each of which can be corrected by an LCWFC. After the correction, three beams are reflected back and received by a camera as a combined beam. Using this method, the light with a waveband of 520–810 nm can be corrected in the whole spectral range with multi-LCWFCs. Furthermore, this method which utilizes multi-LCWFCs to correct the same layer of atmospheric turbulence, should not be used as multi-conjugate adaptive optics to correct the different layers of turbulence. For the adaptive correction with a narrow waveband, the energy outside of this waveband will be lost. Consequently, the energy utilization ratio of the LC AOS can be significantly improved with a wide waveband correction. Compared with Stockley's method, the drawbacks of the non-dispersive LCWFCs do not exist because ordinary LCWFCs were used in our method.

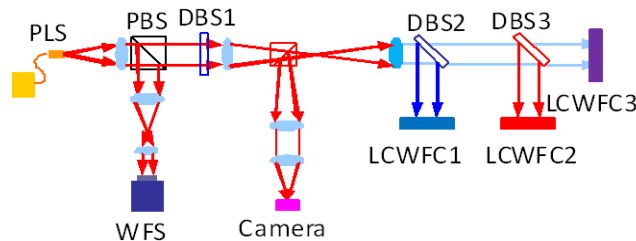


Fig. 4. Optical set-up for broadband correction; PLS represents a point light source, PBS is a polarized beam splitter, DBS means dichroic beam splitter, DBS1 is a bandpass filter, and DBS2 and DBS3 are long-pass filters.

3.2 Static correction

In order to validate our method, a broadband correction experiment was performed with two LCWFCs based on open-loop control. Compared with the optical layout in Fig. 4, the LCWFC3 was removed from the experimental set-up (Fig. 5), and a white light outputting from a fiber bundle was used as a point light source. Owing to computer limitation, only two LCWFCs were used to correct the distortions with the sub-wavebands of 520–590 nm and 590–690 nm. The electronic interface of the LCWFC is PCI Express × 4. Currently, the mainboard can supply three of these interfaces. However, because an NVIDIA GeForce GTX 260 graphic card was used to perform the computation [1] and this covered a PCI Express × 4 interface of the mainboard, only two interfaces can be used to insert the driving card of the LCWFC. Both LCWFCs have an aperture of 7.68 mm × 7.68 mm, 512 pixels × 512 pixels,

and a 200 Hz switching frequency. The WFS consists of 400 microlenses and has a 3 mm aperture; it also has a 500 Hz acquisition frequency.

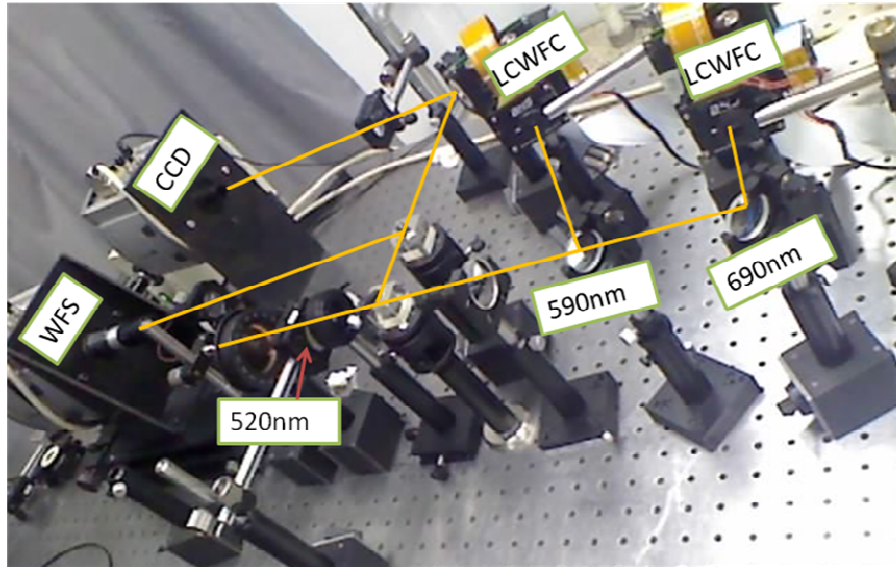


Fig. 5. Optical layout for waveband of 520–690 nm correction with two LCWFCs.

Before the adaptive correction experiment was conducted, the aberration of the LCWFC and LC AOS was tested. The flatness of the LCWFC was measured by using a ZYGO interferometer. It has the root mean square (RMS) value of $\lambda/40$ ($\lambda = 633$ nm), and the reflected wavefront distortion is about $\lambda/20$. After the calibration, the aberration of the LC AOS has an RMS of 0.16λ . Since the LCWFC can correct the distortion with a magnitude of several microns, the aberration of the LC AOS almost had no effect on real-time correction. A US Air Force (USAF) resolution target was placed after the fiber bundle to evaluate the correction effects in a broad waveband. Firstly, the waveband of 520–590 nm was selected to perform the adaptive correction. Figure 6(a) and 6(b) show the images of the resolution target before and after the correction, respectively. After the correction, the second element of the fifth group of the USAF target was resolved, with a resolution of 35.9 cycles/mm; therefore, the resolution ability is 27.9 μm . Considering that the entrance pupil of the optical set-up is 7.7 mm, the diffraction-limited resolution is 26.4 μm for the wavelength of 550 nm. Thus, it can be said that a near diffraction-limited resolution has been achieved after the correction. Figure 6(c) shows the resolving ability for the waveband of 590–690 nm where the distortion was corrected using the other LCWFC. As can be seen, the first element of the fifth group was resolved, and the resolution is 32 cycles/mm. Hence, the resolution is 31.25 μm , which is near the diffraction-limited resolution of 30.4 μm for 633-nm wavelength. In addition, the distortions of two sub-wavebands were corrected at the same time using two LCWFCs. A broadband correction of 520–690 nm was realized, and the corrected result is shown in Fig. 6(d). It can be seen that the first element of the fifth group can also be resolved. These results show that a near diffraction-limited resolution of an optical system can be obtained by using multi-LCWFCs.

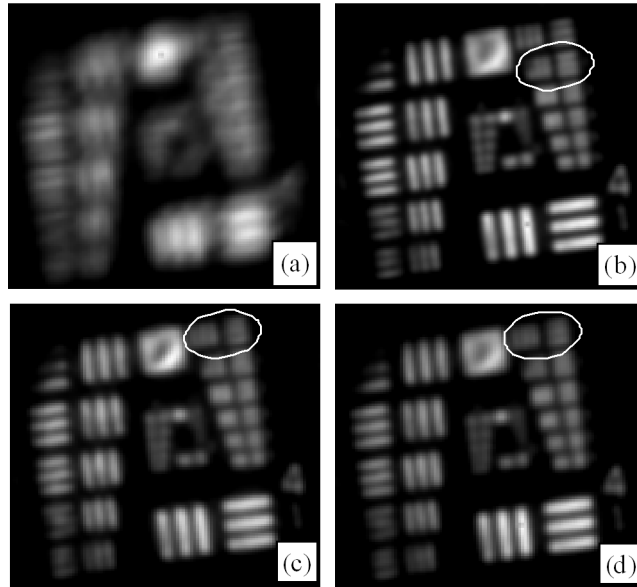


Fig. 6. Images of the resolution target for different wavebands: (a) no correction; (b) 520–590 nm; (c) 590–690 nm; (d) 520–690 nm; the circular area represents the resolving limitation.

Using multi-LCWFCs, the energy utilization ratio of the LC AOS was also considered. The different light sources have different spectral characteristics, which will affect the evaluation of the system energy. Therefore, the spectral curve of the light source used in this experiment was measured, as shown in Fig. 7. It can be seen that at the range of 520–690 nm, the intensity almost did not change. Consequently, image brightness is mainly determined by the spectrum width, and the energy utilization ratio of the LC AOS with two LCWFCs will be

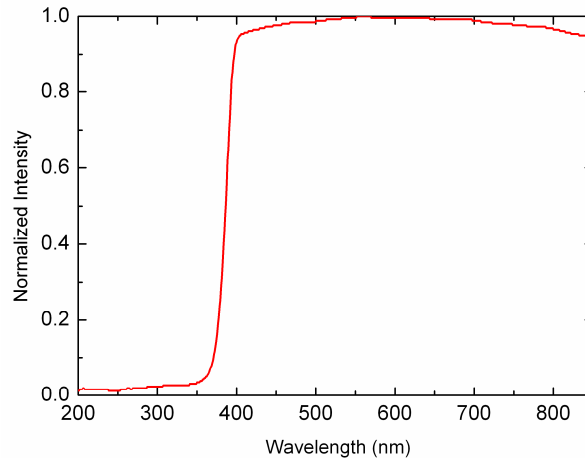


Fig. 7. The spectral curve of the light source.

higher than that with only one LCWFC. All the images in Fig. 6 have the same brightness due to the adjustment in the exposure time of the CCD camera. Actually, the image in Fig. 6(d) has higher brightness than the others. To evaluate the brightness change, the exposure time and gain of the CCD camera were fixed and the brightness of the three images at 520–590 nm, 590–690 nm, and 520–690 nm was recorded. To observe the brightness change clearly, the intensity distribution on a line of the two-dimensional image is plotted in Fig. 8. The

measured data show that when the maximum intensity of 520–690 nm is assumed to be 1, the maximum intensities of 520–590 nm and 590–690 nm are 0.41 and 0.6, respectively. Furthermore, the sum intensity of the 520–590 nm and 590–690 nm wavebands is much closer to the measured intensity of 520–690 nm. This illustrates that the intensity of 520–690 nm is equal to the sum of 520–590 nm and 590–690 nm. Therefore, it can be said that our method is effective in extending the waveband and improving the energy utilization ratio of the LC AOS.

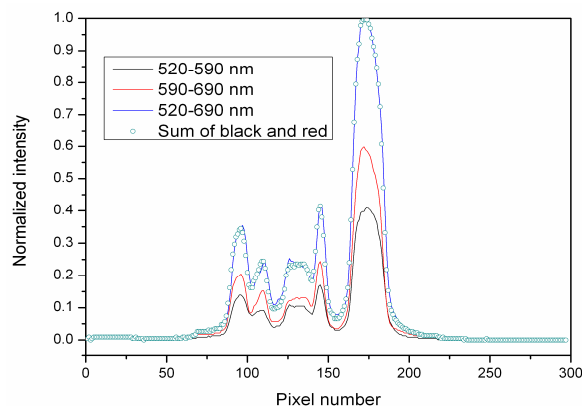


Fig. 8. Brightness distribution in a line of the image: black line, 520–590 nm; red line, 590–690 nm; blue line, 520–690 nm, and the circle represents the sum of the black line and the red line.

3.3 500 m horizontal turbulence correction

Dynamic correction was also performed for the 520–690 nm broadband. A white light source with a fiber bundle output and an off-axis parabolic mirror combination was placed 500 m away to act as an infinite object. A telescope with an aperture of 400 mm was used to observe the object. An LC AOS was placed next to the telescope for horizontal turbulence correction. The concrete optical layout of the LC AOS is shown in Fig. 9. Similar to the static correction, two LCWFCs were used to correct the corresponding sub-waveband. A tip-tilt mirror was utilized to correct the tip-tilt aberration of the horizontal turbulence. The loop frequency of the LC AOS is 80 Hz, and open-loop control was applied. The fiber bundle images with and without adaptive corrections in the spectral range of 520–690 nm are shown in Fig. 10. With the adaptive correction, the resolution of the system is significantly improved and the image of the fiber bundle is clearly resolved. Compared with the original image of the fiber bundle [Fig. 10(a)], the resolution of the corrected image is similar to the original, but the contrast is lower. Since the experiment was performed during daytime, concentration of sunlight on the telescope degraded the contrast of the image. The energy of the LC AOS was also measured using the same method as that of the static correction. Figure 11 shows the intensities for the wavebands of 520–590 nm, 590–690 nm, and 520–690 nm. The measured results indicate that the intensities of 520–590 nm and 590–690 nm are 41% and 59.6% of the 520–690 nm. This illustrates that the system energy was apparently improved with the increase in the waveband. Thus, the correction on the broadband has been demonstrated successfully.

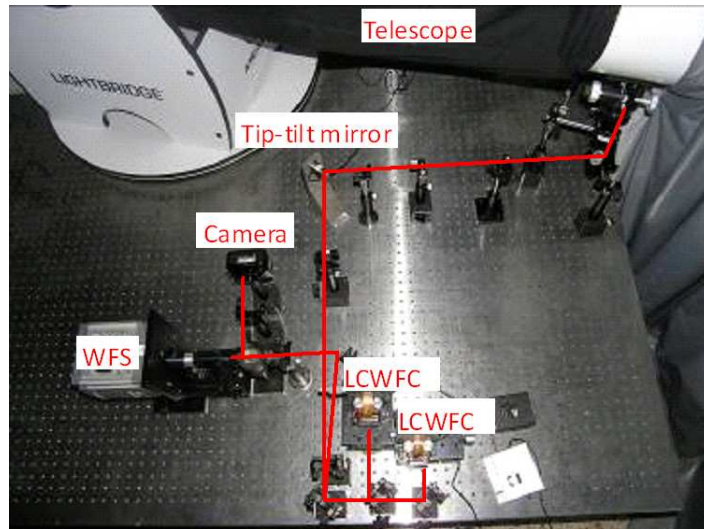


Fig. 9. Optical configuration of the LC AOS.

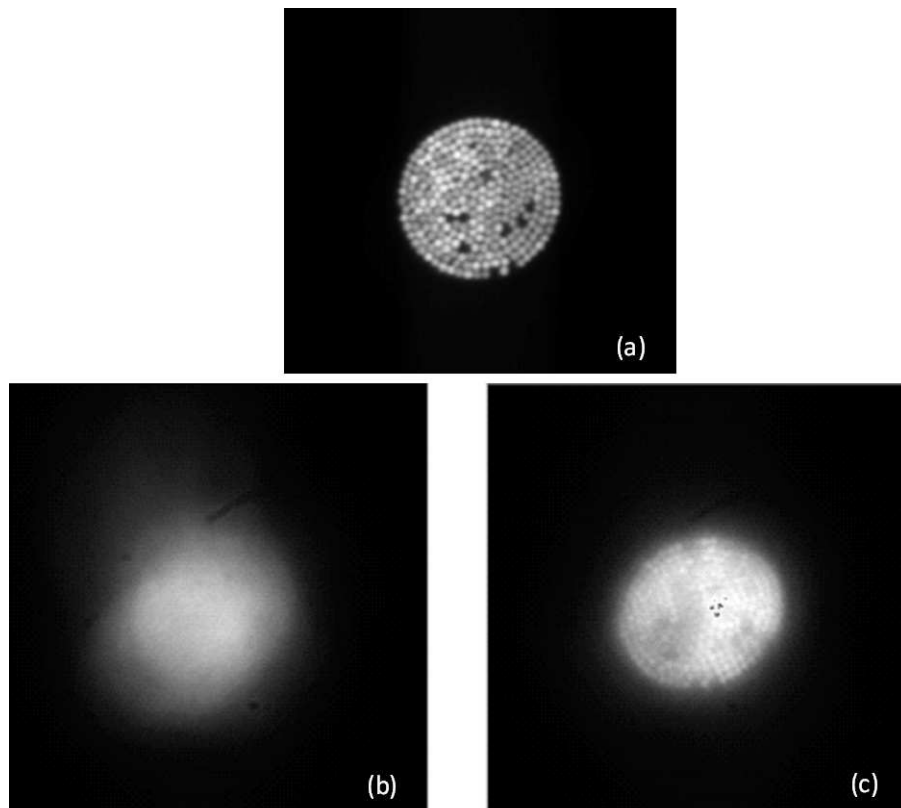


Fig. 10. Fiber bundle image: (a) original image; (b) before correction; (c) after correction.

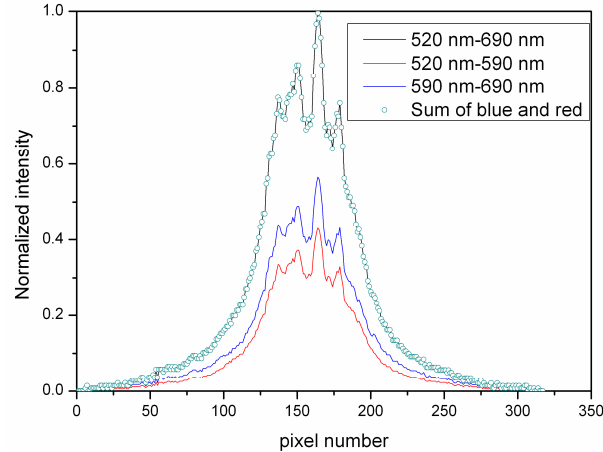


Fig. 11. Brightness distribution in a line of the image: black line, 520–690 nm; red line, 520–590 nm; blue line, 590–690 nm; the circle represents the sum of the black line and the red line.

4. Conclusions

In summary, we have demonstrated a novel method that can extend the working waveband of LC AOS, thereby improving its light efficiency by using multi-LCWFCs. Compared with Stockley's method, the new method has enough phase levels, needs no circular polarization light, and is easy to realize. Firstly, the chromatism of LCWFC was analyzed, and three suitable wavebands were defined. Afterwards, a broadband correction scheme was suggested using multi-LCWFCs. A static correction experiment was performed in the waveband of 520–690 nm. The correction results show that the waveband can be extended by using multi-LCWFCs, with the system energy being approximately of linear proportion to the waveband. Lastly, a 500 m horizontal turbulence was also corrected with the same LC AOS, obtaining similar results. These results indicate that our method can be used for broadband correction to significantly improve the energy utilization ratio of the LC AOS.

Acknowledgement

This work is supported by the National Natural Science Foundation of China, with grant numbers 60736042, 60578035, and 50703039.